Hydraulic tomography of discrete networks of conduits and fractures in a karstic aquifer by using a deterministic inversion algorithm

P. Fischer, Abderrahim Jardani, N. Lecoq

Research Paper/

Hydraulic Tomography of Discrete Networks of Conduits and Fractures in a Karstic Aquifer by Using a Deterministic Inversion Algorithm

P. Fischer[1], A. Jardani[1], N. Lecoq[1]

(1) Normandie Univ, UNIROUEN, UNICAEN, CNRS, M2C, 76000 Rouen, France

Conflict of interest: None

Corresponding author: P. Fischer

E-mail : pierre.fischer1@univ-rouen.fr

Key words: Distributed modeling, Coupled discrete-continuum model, Deterministic inversion, Heterogeneity, Aquifer characterization

Intended for publication in Advances in Water Resources

Abstract

In this paper we present a novel inverse modeling method called Discrete Network Deterministic Inversion (DNDI) for mapping the geometry and property of the discrete network of conduits and fractures in the karstified aquifers. The DNDI algorithm is based on a coupled discrete-continuum concept to simulate numerically water flows in a model and a deterministic optimization algorithm to invert a set of observed piezometric data recorded during multiple pumping tests. In this method, the model is partioned in subspaces piloted by a set of parameters (matrix transmissivity, and geometry and equivalent transmissivity of the conduits) that are considered as unknown. In this way, the deterministic optimization process can iteratively correct the geometry of the network and the values of the properties, until it converges to a global network geometry in a solution model able to reproduce the set of data. An uncertainty analysis of this result can be performed from the maps of posterior uncertainties on the network geometry or on the property values. This method has been successfully tested for three different theoretical and simplified study cases with hydraulic responses data generated from hypothetical karstic models with an increasing complexity of the network geometry, and of the matrix heterogeneity.

1. Introduction

In hydrogeological studies, the choice of the management and protection strategies of the groundwater resources is mainly based on the characterization of the hydraulic properties of the aquifer, such as hydraulic conductivity and specific storage. This characterization is most often carried out from pumping, slug and tracer tests by intrusively recording the aquifer responses, such as hydraulic pressure and tracer concentration at a set of boreholes (Butler 2005). The reliability of these techniques for capturing the spatial heterogeneity of the hydrodynamic properties is particularly conditioned by the amount and spatial disposition of wells used during the investigation, and the procedure applied to analyze the hydraulic data (Yeh and Lee 2007). In karstic and/or fractured aquifers the hydrodynamic properties (such as the hydraulic conductivity) can vary significantly from 10^{-10} m/s to 10^{-1} m/s, even at small scales (Wang et al. 2016). This heterogeneity mainly depends on the apertures, connectivity and density of the conduits and fractures network in the medium, making the groundwater flow path complex (Eisenlohr et al. 1997 ; Kovacs et al. 2005 ; Borghi et al. 2016 ; Ronayne 2013). In this complex context, the hydraulic flow pattern is spatially disconnected and principally focused in the transmissive fissures and fractured zones, wherein the geometrical features and hydraulic flow regime (turbulent or laminar) are usually difficult to identify, especially with a limited number of wells, or with the use of oversimplified assumptions for interpreting the piezometric data to infer the hydrodynamic parameters.

In the hydroscience literature, several different modeling approaches based on the physical theories have already been tested in order to simulate the dynamics of karstic flows for the prediction of hydraulic properties (Hartmann et al. 2014). Among them, the equivalent porous media model, also called the single continuum model, in which the discrete features of fractures and karstic conduits are conceptualized as a porous media with continuous hydraulic properties (Larocque et al. 1999 ; Illman 2014 ; Wang et al. 2016). This simplifies the

description of heterogeneity of karstic aquifers because it does not require an accurate knowledge on the architecture of fractures and conduits networks for simulating the groundwater flows. In such concept, it is sufficient to assign high hydraulic conductivity values to fractured zones and very low conductivity for intact rock. Otherwise, the coupled discrete-continuum distributed approach is of great interest thanks to its ability to imitate the dual hydrodynamic behaviors in the fractured aquifers by using Discrete Channel or Fracture Networks (DCN/DFN) for the conduits and fractures, and equivalent porous media for representing the matrix blocks (Teutsch 1993 ; Liedl et al. 2003 ; De Rooij et al. 2013). In contrast to the equivalent porous media model, the discrete-continuum approach requires a good knowledge on the geometry of the karstic and fracture networks. The influence of the discrete network geometry on the hydraulic simulations and the benefits of a coupled discrete-continuum approach compared to the equivalent porous media have been widely discussed in the literature (Kovacs 2003 ; Painter and Cvetkovic 2005 ; Ghasemizadeh et al. 2012 ; Hartmann et al. 2014). One of these advantages is its efficiency to reproduce numerically the hydraulic fluctuations of karst spring discharge, while an equivalent porous media systematically generated lower values than the ones measured (Kovacs 2003).

The hydraulic tomography is a useful tool to predict rigorously the spatial distribution of the hydraulic properties, or the structural architecture of the fractures and conduits and their properties. It involves the use of inverse algorithms to analyze jointly a set of hydraulic data collected during multiple pumping tests (Carrera et al. 2005 ; Cliffe et al. 2011 ; Zhou et al. 2014). In this framework, various inversion algorithms were successfully applied for characterizing the hydraulic properties of fractured and heterogeneous aquifers using both concepts of parametrization discussed in the previous paragraph: the equivalent porous media and coupled discrete-continuum approach.

(1) Inversions in an equivalent porous media were led by using geostatistical approaches in which the statistical characteristics of hydraulic properties are used as a priori information to constraint the inversion. Among these tools we cite: sequential successive linear estimator (Yeh and Liu 2000 ; Ni and Yeh 2008 ; Hao et al. 2008 ; Illman et al. 2009 ; Sharmeen et al. 2012), pilot-point (Lavenue and de Marsily 2001), transitional-probability (Wang et al. 2017), anisotropy directions (Meier et al. 2001), multi-scale resolution (Ackerer and Delay 2010), or structural approaches: probability perturbation method (Caers and Hoffman 2006), image-guided (Soueid Ahmed et al. 2015), and cellular automata-based (Fischer et al. 2017).

(2) On the other hand, the parameterization of hydraulic tomography using a distributed discrete-continuum approach is less flexible than the concept of the equivalent porous medium because the discrete-continuum model relies on the establishment of the architecture of the conduits and fractures, and their hydraulic properties. Several works have already brought some solutions to these difficulties. One solution would be to generate stochastically patterns of networks with various constraints: statistical constraints (Li et al. 2014 ; Le Coz et al. 2017), mechanical constraints (Bonneau et al. 2013 ; Jaquet et al. 2004), geological and speleogeological metrics information (Collon et al. 2017 ; Pardo-Iguzquiza et al. 2012), or flows hierarchical identification (Le Goc et al. 2010). More recently, Borghi et al. (2016) have combined the use of a generator of karstic networks, based on sets of fractures stochastically generated, with a gradient-based parameters optimization in order to reconstruct a discrete network able to reproduce a set of tracer test hydraulic data.

In this present article we propose a novel strategy for dealing with hydraulic tomography of fractured and karstic aquifers, which we will shorten as the Discrete Network Deterministic Inversion (DNDI). The DNDI algorithm permits to map the architecture of fractures and conduits networks, their hydraulic properties, and the distribution of the transmissivity in the hard rock (matrix).

The DNDI approach relies on the use of a coupled discrete-continuum concept to simulate water flows through a karstic and fractured aquifer and a deterministic optimization algorithm to invert a set of observed piezometric data recorded during multiple pumping tests. The model is partitioned in several subspaces, each one being piloted locally by a set of parameters including: the orientations of the conduit/fracture, their equivalent transmissivity values, and the transmissivity of the rock matrix. This partitioning makes it possible to locally modify the directions of the fracture network and to iteratively update the geometry of the global network in order to minimize the objective function in the inverse process. The method is tested on several hypothetical and simplified karstic aquifers with simple to more complex conduit networks and with homogeneous or heterogeneous transmissivity in the matrices.

2. Algorithm framework

2.1. Forward problem and model parameterization

We represent a confined karstic and fractured aquifer in a two-dimensional model Γ with an equivalent porous media Γ_M (for representing the water flows where the rock is intact) and a discrete network Γ_N (for simulating the water flows in the fracture/conduit networks). The numerical simulation of groundwater flows are governed by a steady state continuity equation associated to Darcy's law, considering a laminar flow in both the matrix domain and the discrete networks:

$$\begin{cases} \nabla.(-e_M K_M.\nabla \mathrm{h}) = \dfrac{e_M Q_M}{\mathcal{V}_{\mathrm{el.}}} & \text{in the matrix } \Gamma_M \\ \nabla_T.(-e_N K_N.\nabla_T \mathrm{h}) = \dfrac{e_N Q_N}{\mathcal{V}_{\mathrm{el.}}} & \text{in the network } \Gamma_N \end{cases} \quad (1)$$

where Q_M and Q_N are punctual water extraction or injection rates per unit of thickness ($m^3/s/m$) applied on the matrix and network respectively, K_M denotes the matrix hydraulic

conductivities (m/s), K_N denotes the fractures or conduits equivalent conductivities (m/s), h is the piezometric level (m) common to both domains Γ_M and Γ_N, e_M (m) is the thickness of the matrix block, e_N (m) is the aperture of the network, and $\mathcal{V}_{el}$ is an elementary volume at the pumping location (m^3). We mention that Darcy's law formulation in the matrix domain is described in 2D, and in 1D for fractured networks at the internal network boundaries. That's why we use the tangential gradient operator $\nabla_T = \vec{\nabla}.\vec{\ell}$ (where $\vec{\ell}$ is a local directional unit vector of the network) to solve the hydraulic equation at the network. In the study cases presented later in this article, we have chosen to simulate laminar flows as presented in Eq. 1 in a network of conduits. However, the property values K_N in the network can be more specifically adapted to the behavior of turbulent conduit flows or fracture flows through other empirical laws (eventually related to an aperture variable).

The forward problem consists in solving numerically Eq. 1 by using a finite element technique with a triangular meshing. It links the hydraulic head data simulated continuously over the coupled model to the spatial distribution in the model of the conduits or fractures with their properties in 1D, and the hydraulic transmissivities of the matrix in 2D (Figure 1). The forward problem can be formulated as:

$$\mathbf{d} = f\left(\mathbf{\Gamma}\left(\mathbf{P_{Dir}}, \mathbf{P_{Prop}}\right)\right) + \boldsymbol{\varepsilon} \ , \tag{2}$$

where $\mathbf{d}$ is a vector of simulated hydraulic data $(n \times 1)$, f is a forward operator that calculates the hydraulic data field from a model $\mathbf{\Gamma}\left(\mathbf{P_{Dir}}, \mathbf{P_{Prop}}\right)$ defined by given parameters of network geometry $\mathbf{P_{Dir}}$ and hydraulic properties $\mathbf{P_{Prop}}$, $\boldsymbol{\varepsilon}$ is a null mean Gaussian noise to add the uncertainties associated to the numerical discretization technique and the hydraulic experimental data. The model is enclosed in a large buffer zone associated to an equivalent porous media mean transmissivity. This zone permits to limit the influence of the boundary

conditions. The DNDI inversion algorithm was coded using Matlab and is linked to the COMSOL Multiphysics software which runs the forward problems.

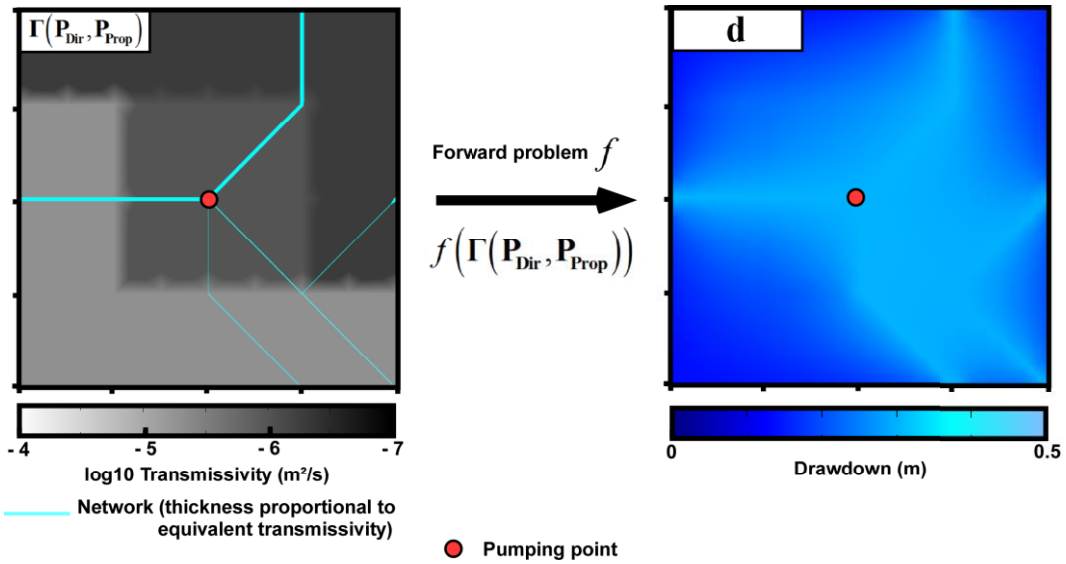

Figure 1: Example of a simulated distribution of hydraulic heads (here drawdowns) by solving the forward problem f (Eq.1) for a steady state pumping in a given coupled discrete-continuum distributed model $\mathbf{\Gamma}(\mathbf{P}_{Dir}, \mathbf{P}_{Prop})$.

For the DNDI algorithm, the model domain $\mathbf{\Gamma}$ is partitioned in p_x squared subspaces along the X-axis and p_y along the Y-axis. The total of subspaces of the whole domain is then $p = p_x \times p_y$. Three parameters are assigned to each subspace (Figure 3):

(1) the local direction of the conduit/fracture network,

(2) the local conduit/fracture equivalent transmissivity value,

(3) and the local matrix transmissivity value.

The geometry of the network follows the local direction in each subspace by a node-to-node principle. The network structure enters a subspace by activating one of its four nodes (corners of the square) and the subspace direction parameter will define to each other node of the

subspace the structure will generate. This other node will then be activated itself and permits to the structure to include new subspaces. A subspace in which the structure has already been generated becomes inhibited to another generation from the same network. The generation process is schematized in Figure 2.

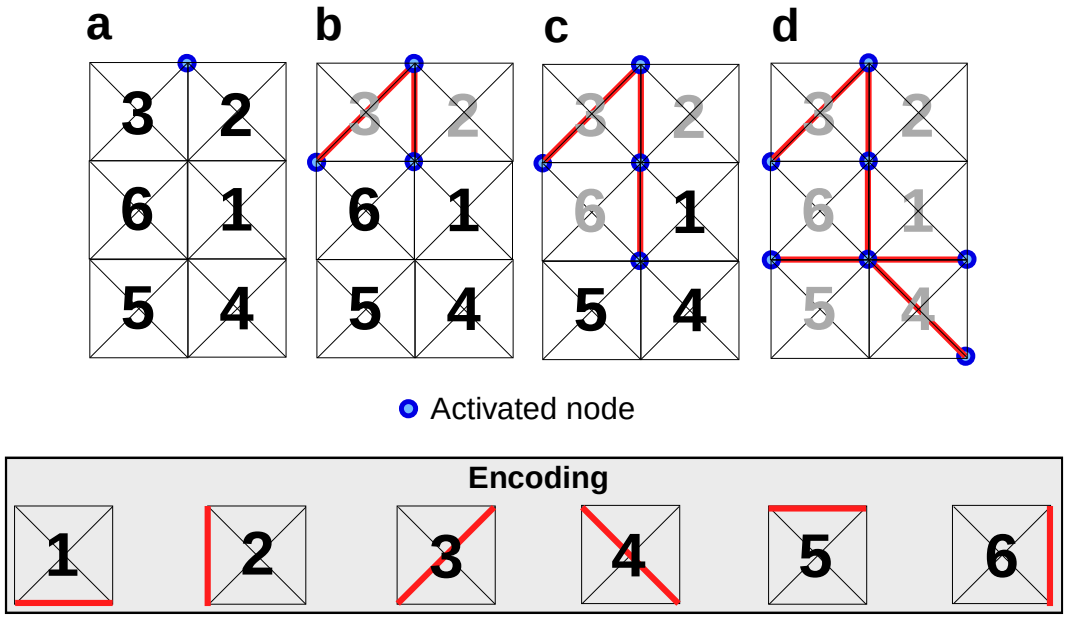

Figure 2: Schema of the node-to-node generation process in the DNDI method with six subspaces. An activated node in the top subspaces (a) starts the generation of the structure. The structure generates to the nodes in the bottom of these subspaces, following the local direction defined in the subspaces through the encoding rules. These reached nodes then become activated (b). The subspaces in which the structure has generated become inhibited to another generation (shown as greyed number in this figure). The structure then continues its generation from its newly activated node if the subspaces structural parameters permit it (c) – (d).

In order to perform this node-to-node generation, an initially activated node has to be specified in the model (starting node in Figure 3). The model geometry in COMSOL is built as a discrete grid including all network possibilities (a grid of squares and diagonals as presented in Figure 3). This whole geometry is initially disabled in the COMSOL physical part. When different network geometries are tested in the inversion process, only the associated parts in the model grid are enabled for the solver computation. This avoids the

creation of a new model geometry for each modification of the network and permits to reduce the computing time in the inversion.

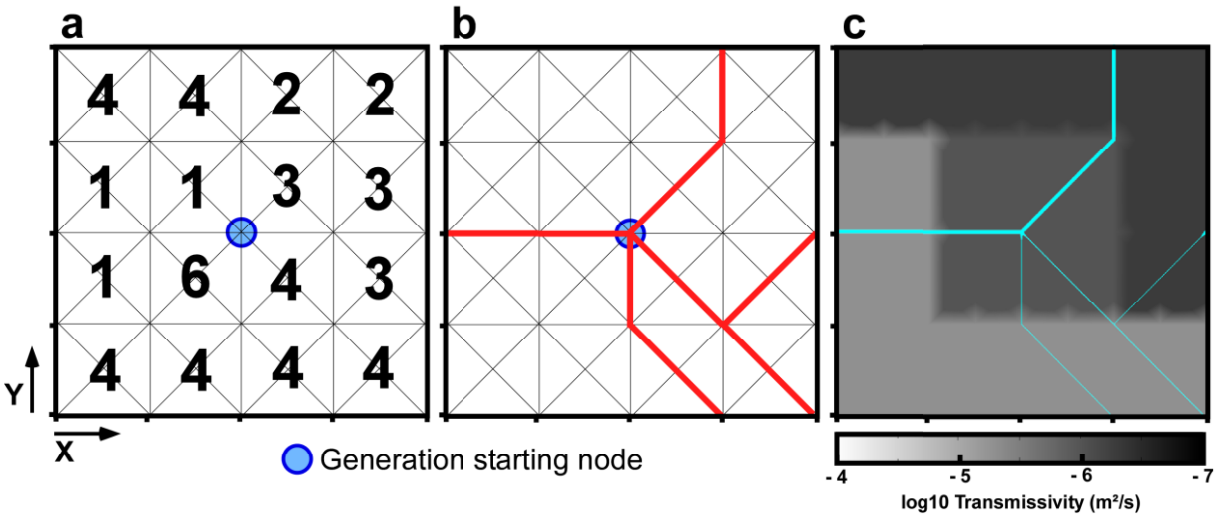

Figure 3: Parameterization of a model in the DNDI method. For each subspace of the model there are six local direction possibilities (see encoding in Figure 2) that are used to parameterize a network structure in the model (a). The structure (in red) is then generated, following a node-to-node rule, from the set of structural parameters in (a) and a chosen starting point at a node between subspaces (b). Finally a set of property values (transmissivities), also defined for each subspace, is assigned to the structural model (c).

The parameterization of the whole model is contained in two vectors piloting the subspaces.

(1) The local direction in a subspace is selected among six possibilities (see Figure 3) as a structural parameter $\mathrm{Dir} \in \{1,2,3,4,5,6\}$. The set of structural parameters for all subspaces in the model is contained in a $(p \times 1)$ vector $\mathbf{P}_{\mathbf{Dir}}$. It is also possible to generate more than one network, but this would add more unknown structural parameters. For example if one would want to generate 3 independent networks in the model, each subspace would need to define 3 local directions instead of one. Thus, the structural vector of direction parameters $\mathbf{P}_{\mathbf{Dir}}$ would become a $(3p \times 1)$ vector.

189 (2) The local equivalent transmissivity of the structure in a subspace is defined as a property
190 parameter T_N and the matrix transmissivity as a property parameter T_M. The set of property
191 parameters for all subspaces in the model is contained in a $(2p \times 1)$ vector $\mathbf{P_{Prop}}$ with the p
192 parameters T_N followed by the p parameters T_M. The entire model $\mathbf{\Gamma}$ is thus piloted only
193 by two parameter vectors: $\mathbf{P_{Dir}}$ and $\mathbf{P_{Prop}}$, and can be noted $\mathbf{\Gamma}\left(\mathbf{P_{Dir}}, \mathbf{P_{Prop}}\right)$.

194 ## 2.2. Inverse problem

195 The inversion process in the DNDI algorithm consists in retrieving a model of network of
196 conduit/fracture and of spatial distribution of the transmissivities of the network and matrix
197 which permits to maximize two probability density functions ρ_{network} and $\rho_{\text{properties}}$. Following
198 the theory described by Tarantola and Valette (1982) for a least square criterion resolution of
199 the inverse problem, we calculate ρ_{network} and $\rho_{\text{properties}}$ with the Bayes theorem, by considering
200 Gaussian laws for the probability density functions ρ, and $\rho(\mathbf{d}_{\text{obs}})$ as certain:

$$\rho_{\text{network}}\left(\mathbf{P_{Dir}}\middle|\mathbf{d}_{\text{obs}}, \mathbf{P_{Prop}}\right) = \rho\left(\mathbf{d}_{\text{obs}}\middle|\mathbf{P_{Dir}}, \mathbf{P_{Prop}}\right).\rho\left(\mathbf{P_{Dir}}\right) / \rho\left(\mathbf{d}_{\text{obs}}\right)$$

201
$$\rho_{\text{network}}\left(\mathbf{P_{Dir}}\middle|\mathbf{d}_{\text{obs}}, \mathbf{P_{Prop}}\right) \propto exp\left(-\frac{1}{2}\left(\mathbf{d}_{\text{obs}} - f\left(\mathbf{\Gamma}\left(\mathbf{P_{Dir}}, \mathbf{P_{Prop}}\right)\right)\right)^{\mathrm{T}} \mathbf{C}_{\mathrm{d}}{}^{-1}\left(\mathbf{d}_{\text{obs}} - f\left(\mathbf{\Gamma}\left(\mathbf{P_{Dir}}, \mathbf{P_{Prop}}\right)\right)\right)\right)$$
$$\times exp\left(-\frac{1}{2}\left(\mathbf{P_{Dir,prior}} - \mathbf{P_{Dir}}\right)^{\mathrm{T}} \mathbf{C}_{\mathbf{P_{Dir}}}{}^{-1}\left(\mathbf{P_{Dir,prior}} - \mathbf{P_{Dir}}\right)\right)$$

202 (3)

$$\rho_{\text{properties}}\left(\mathbf{P_{Prop}}\middle|\mathbf{d}_{\text{obs}}, \mathbf{P_{Dir}}\right) = \rho\left(\mathbf{d}_{\text{obs}}\middle|\mathbf{P_{Prop}}, \mathbf{P_{Dir}}\right).\rho\left(\mathbf{P_{Prop}}\right) / \rho\left(\mathbf{d}_{\text{obs}}\right)$$

203
$$\rho_{\text{properties}}\left(\mathbf{P_{Prop}}\middle|\mathbf{d}_{\text{obs}}, \mathbf{P_{Dir}}\right) \propto exp\left(-\frac{1}{2}\left(\mathbf{d}_{\text{obs}} - f\left(\mathbf{\Gamma}\left(\mathbf{P_{Dir}}, \mathbf{P_{Prop}}\right)\right)\right)^{\mathrm{T}} \mathbf{C}_{\mathrm{d}}{}^{-1}\left(\mathbf{d}_{\text{obs}} - f\left(\mathbf{\Gamma}\left(\mathbf{P_{Dir}}, \mathbf{P_{Prop}}\right)\right)\right)\right)$$
$$\times exp\left(-\frac{1}{2}\left(\mathbf{P_{Prop,prior}} - \mathbf{P_{Prop}}\right)^{\mathrm{T}} \mathbf{C}_{\mathbf{P_{Prop}}}{}^{-1}\left(\mathbf{P_{Prop,prior}} - \mathbf{P_{Prop}}\right)\right)$$

204 (4)

where $\propto$ represents a proportionality relation, $\rho_{\text{network}}\left(\mathbf{P_{Dir}}\middle|\mathbf{d}_{\text{obs}},\mathbf{P_{Prop}}\right)$ represents the a posteriori probability density function of the discrete fracture network model for a given hydraulic observed data $\mathbf{d}_{\text{obs}}$ and the transmissivity model of the network and matrix $\mathbf{P_{Prop}}$. $\rho_{\text{properties}}\left(\mathbf{P_{Prop}}\middle|\mathbf{d}_{\text{obs}},\mathbf{P_{Dir}}\right)$ is the a posteriori probability density function of the spatial distribution of the transmissivity parameters for a given hydraulic observed data $\mathbf{d}_{\text{obs}}$ and network model $\mathbf{P_{Dir}}$. $\rho\left(\mathbf{d}_{\text{obs}}\middle|\mathbf{P_{Dir}},\mathbf{P_{Prop}}\right)$ and $\rho\left(\mathbf{d}_{\text{obs}}\middle|\mathbf{P_{Prop}},\mathbf{P_{Dir}}\right)$ represent the probability density functions of the network structure and property models, which permit to evaluate the ability of the network structure and property models to reproduce the observed data via the use of the forward operator. $\rho\left(\mathbf{P_{Dir}}\right)$ and $\rho\left(\mathbf{P_{Prop}}\right)$ represent prior distributions for the unknown parameters. It is well known that, on one hand, the piezometric data are insufficient to cope with the non-uniqueness of the solution of an inverse process, and on another hand, that a deterministic inversion process leads to a single local solution dependent to the initial model. For these reasons, and in order to additionally constrain the inversion to a more realistic solution in relation to the field knowledges, it can be interesting to incorporate prior distributions for the unknown parameters in $\rho\left(\mathbf{P_{Dir}}\right)$ and $\rho\left(\mathbf{P_{Prop}}\right)$.

The maximization of the a posteriori probability density functions ρ_{network} and $\rho_{\text{properties}}$ is equivalent to a minimization of the arguments of the exponentials in Eq.3 and 4. This is what we aim to minimize during the inversion process in the following objective functions Ψ:

$$\begin{aligned}\Psi_{\text{network}}\left(\mathbf{P_{Dir}}\right) = &\frac{1}{2}\left(\mathbf{d}_{\text{obs}} - f\left(\mathbf{\Gamma}\left(\mathbf{P_{Dir}},\mathbf{P_{Prop}}\right)\right)\right)^{\mathrm{T}}\mathbf{C}_{\mathrm{d}}{}^{-1}\left(\mathbf{d}_{\text{obs}} - f\left(\mathbf{\Gamma}\left(\mathbf{P_{Dir}},\mathbf{P_{Prop}}\right)\right)\right)\\ &+\frac{1}{2}\left(\mathbf{P}_{\mathbf{Dir},\text{prior}} - \mathbf{P_{Dir}}\right)^{\mathrm{T}}\mathbf{C}_{\mathbf{P_{Dir}}}{}^{-1}\left(\mathbf{P}_{\mathbf{Dir},\text{prior}} - \mathbf{P_{Dir}}\right)\end{aligned} \tag{5}$$

$$\Psi_{\text{properties}}\left(\mathbf{P_{Prop}}\right)=\frac{1}{2}\left(\mathbf{d}_{\text{obs}}-f\left(\Gamma\left(\mathbf{P_{Dir}},\mathbf{P_{Prop}}\right)\right)\right)^{\text{T}}\mathbf{C}_{\text{d}}{}^{-1}\left(\mathbf{d}_{\text{obs}}-f\left(\Gamma\left(\mathbf{P_{Dir}},\mathbf{P_{Prop}}\right)\right)\right)+\frac{1}{2}\left(\mathbf{P}_{\mathbf{Prop},\text{prior}}-\mathbf{P_{Prop}}\right)^{\text{T}}\mathbf{C}_{\mathbf{P_{Prop}}}{}^{-1}\left(\mathbf{P}_{\mathbf{Prop},\text{prior}}-\mathbf{P_{Prop}}\right) \quad (6)$$

where $\mathbf{d}_{\text{obs}}$ is a vector of observed data $(n\times 1)$, $\mathbf{P_{Dir}}$ and $\mathbf{P_{Prop}}$ are the unknown parameters to estimate for imaging the geometry of the network (in $\mathbf{P_{Dir}}$) and the hydraulic properties (defined here by the equivalent transmissivity of the conduits/fractures and the transmissivity of the matrix in $\mathbf{P_{Prop}}$). $\mathbf{P}_{\mathbf{Dir},\text{prior}}$ $(p\times 1)$ and $\mathbf{P}_{\mathbf{Prop},\text{prior}}$ $(2p\times 1)$ are the prior information on the geometry and on the property parameters employed to constrain the inverse problem for overcoming the unrealistic solutions, $\mathbf{C}_{\text{d}}$ $(n\times n)$ is a covariance matrix on the observed data that permits to include the uncertainties of the hydraulic data in the inversion process. $\mathbf{C}_{\mathbf{P_{Dir}}}$ $(p\times p)$ and $\mathbf{C}_{\mathbf{P_{Prop}}}$ $(2p\times 2p)$ are the covariance matrices on the structural and property parameters respectively.

This separated formulation of the probability density functions between network and properties permits to sequentially estimate the two dependent unknown models $\mathbf{P_{Dir}}$ and $\mathbf{P_{Prop}}$. In a first step, we focus on the characterization of the network with the piezometric data by fixing the model of the transmissivity distributions in the conduits/fractures and matrices. The model of network resulting from the first step will then be used in a second step as known parameter to infer the transmissivity pattern.

2.3. Optimization and uncertainty analysis

The minimization of Eq. 5 and Eq. 6 can be done by optimizing the network geometry and the property values during two sequential iterative processes. These optimizations consist in successively modifying the structural and property parameters $\mathbf{P_{Dir}}$ and $\mathbf{P_{Prop}}$.

The inversion process is led as a sequential optimization (Figure 4) of

245 (1) the structural geometry (considering as fixed the initially chosen property values),

246 (2) and the property values T_N, T_M (considering as fixed the previously inverted structural

247 geometry).

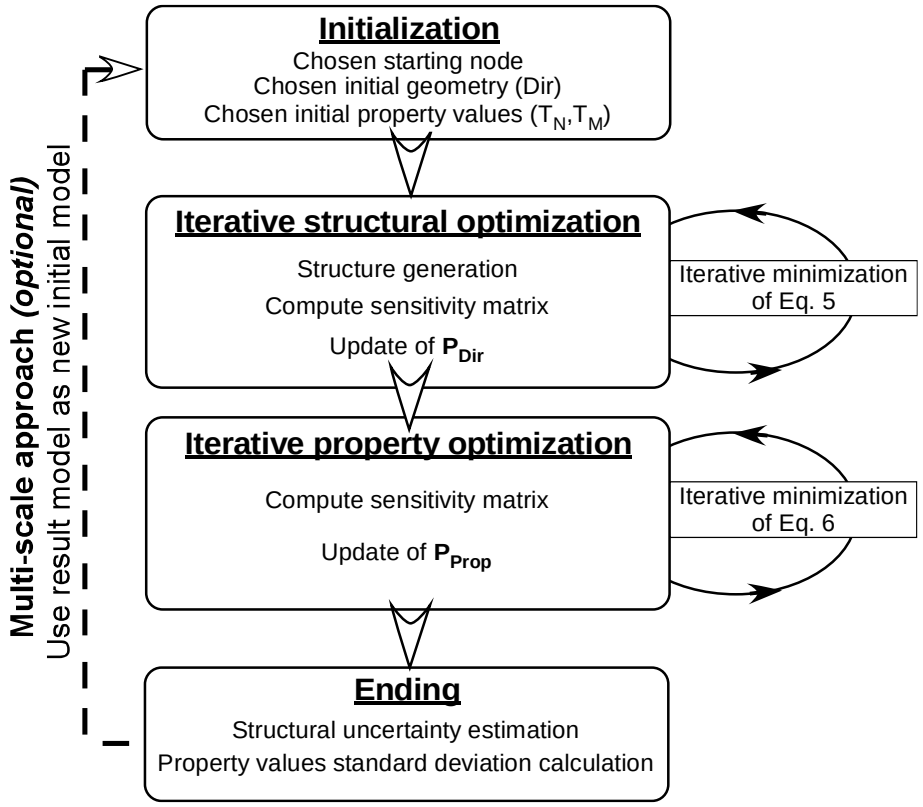

248

249 Figure 4: A flowchart of the inversion steps used in the DNDI algorithm. After the
250 initialization of the parameters, a sequential iterative optimization is led on the structure
251 geometry and on the property values in order to minimize both objective functions (Eq. 5 and
252 Eq. 6). An eventual re-run of the inversion process (multi-scale option) using the result as new
253 initial model can be performed in order to improve this result.

254

255 The structural optimization is performed iteratively by modifying the structural parameter $\mathbf{P_{Dir}}$

256 through a structural sensitivity analysis and by considering the hydraulic properties $\mathbf{P_{Prop}}$ as

257 fixed. At a given iteration step k, the sensitivity analysis of the network geometry toward the

258 observed data is recorded into a $(6 \times p)$ sensitivity matrix $\mathbf{J_n}^k$. For a local direction $i \in [1,6]$

259 and for a subspace $j \in [1, p]$ the element of the matrix $\mathbf{J_n}^k$ is calculated as:

$$\mathbf{J_n}^{k}(i,j)=\frac{1}{2}\left(\mathbf{d}_{obs}-f\left(\mathbf{\Gamma}\left(\mathbf{P}_{\mathbf{Dir}}^{k}\big|_{\mathbf{P_{Dir}}(j)=i},\mathbf{P_{Prop}}\right)\right)\right)^{T}\mathbf{C}_{d}^{-1}\left(\mathbf{d}_{obs}-f\left(\mathbf{\Gamma}\left(\mathbf{P}_{\mathbf{Dir}}^{k}\big|_{\mathbf{P_{Dir}}(j)=i},\mathbf{P_{Prop}}\right)\right)\right)+\frac{1}{2}\left(\mathbf{P}_{\mathbf{Dir},prior}(j)-i\right)^{T}\mathbf{C}_{\mathbf{P_{Dir}}}^{-1}\left(\mathbf{P}_{\mathbf{Dir},prior}(j)-i\right) \quad (7)$$

with $\mathbf{P}_{\mathbf{Dir}}^{k}\big|_{\mathbf{P_{Dir}}(j)=i}$ the structural geometry parameter at the iteration k considering a modified local direction in the subspace j, and $\left(\mathbf{P}_{\mathbf{Dir},prior}(j)-i\right)$ the gap between the prior local direction of subspace j and the modified local direction.

Thus, the sensitivity matrix guides the evolution of the objective function in Eq. 5 by testing successively the modification of the network with all possible local direction in each subspace. The minimal value in the matrix $\mathbf{J_n}^{k}(i_{min},j_{min})$ designates the local direction i_{min} in the subspace j_{min} which would produce the best decrease in the objective function.

Then the parameters set $\mathbf{P_{Dir}}^{k}$ is updated from the previous set $\mathbf{P_{Dir}}^{k}=\mathbf{P_{Dir}}^{k-1}$ by taking into account the sensitivity analysis minimum $\mathbf{P_{Dir}}^{k}(j_{min})=i_{min}$ in order to minimize the objective function at each step of the optimization.

Once the sensitivity analysis cannot find any more $\mathbf{P_{Dir}}$ configuration decreasing the objective function, the iterative structural optimization is stopped. The last structural iteration represents the local solution, dependent to the initial model. The uncertainty analysis of the inverted network geometry can be inferred from the computation of the posterior covariance matrix as:

$$\mathbf{C}_{\mathbf{P_{Dir}}}^{post}(j)=\left(\frac{1}{6}\sum_{i=1}^{6}\mathbf{J_n}^{post}(i,j)-\Psi_{network}^{post}+\mathbf{C}_{\mathbf{P_{Dir}}}^{-1}(j,j)\right)^{-1}, \quad (8)$$

where $\mathbf{C}_{\mathbf{P_{Dir}}}^{post}(j)$ is the posterior structural uncertainty value for the local direction in the subspace j, $\mathbf{J_n}^{post}$ is the last iteration structural sensitivity matrix and $\Psi_{network}^{post}$ is the value of the minimized structural objective function. If the structural uncertainty value is low, then

another direction in the subspace would lead to a deterioration of the reproduction of the data. On the other hand if the structural uncertainty value is high, then the structure in the subspace could have another local direction without significantly degrading the reproduction of the observed data.

Following the network geometry optimization, the property parameters optimization will iteratively modify the transmissivities with the previously inverted geometry in order to minimize the objective function in Eq. 6. The network equivalent transmissivities and the matrix transmissivities are optimized simultaneously. At a given iteration step k, the parameters set $\mathbf{P}_{\mathbf{Prop}}$, which contains the transmissivities for both the network and the matrix, is updated by linearizing Eq. 6, which can be formulated as:

$$\mathbf{P}_{\mathbf{Prop}}^{\mathrm{k+1}} = \mathbf{P}_{\mathbf{Prop}}^{\mathrm{k}} + \left(\left(\mathbf{J}_{\mathbf{p}}{}^{\mathrm{k}}\right)^{\mathrm{T}}.\mathbf{C}_{\mathrm{d}}{}^{-1}.\mathbf{J}_{\mathbf{p}}{}^{\mathrm{k}} + \mathbf{C}_{\mathbf{P}_{\mathbf{Prop}}}{}^{-1}\right)^{-1}.\left(\mathbf{J}_{\mathbf{p}}{}^{\mathrm{k}}\right)^{\mathrm{T}}.\mathbf{C}_{\mathrm{d}}{}^{-1}.\left(\mathbf{d}_{\mathrm{obs}} - f\left(\mathbf{\Gamma}\left(\mathbf{P}_{\mathbf{Dir}}, \mathbf{P}_{\mathbf{Prop}}^{\mathrm{k}}\right)\right)\right) + \mathbf{C}_{\mathbf{P}_{\mathbf{Prop}}}{}^{-1}.\left(\mathbf{P}_{\mathbf{Prop},\mathrm{prior}} - \mathbf{P}_{\mathbf{Prop}}^{\mathrm{k}}\right) \tag{9}$$

where $\mathbf{J}_{\mathbf{p}}{}^{\mathrm{k}}$ is the Jacobian matrix $(n \times 2p)$ that holds the sensitivity for each modeled data f_{i} (at the positions of the observed data) toward the property values in the matrix and the network. This Jacobian matrix can be calculated by using a finite difference approach, with a finite difference step $\mathbf{\Delta P_{Prop}}$:

$$\mathbf{J}_{\mathbf{p}}{}^{\mathrm{k}}\left(\mathrm{i},\mathrm{j}\right) = \left.\frac{\partial f_{\mathrm{i}}}{\partial \mathbf{P}_{\mathbf{Prop}}{}^{\mathrm{k}}}\right|_{\mathbf{P}_{\mathbf{Prop}}{}^{\mathrm{k}}(\mathrm{j})=\mathbf{P}_{\mathbf{Prop}}{}^{\mathrm{k}}(\mathrm{j})+\mathbf{\Delta P}_{\mathbf{Prop}}} . \tag{10}$$

Finally, once the objective function has iteratively converged to a minimum, the property optimization is stopped. The posterior covariance matrix on the inversion of the property values can be calculated as:

$$\mathbf{C}_{\mathbf{P}_{\mathbf{Prop}}}^{post} = \left(\left(\mathbf{J}_{\mathbf{p}}{}^{post}\right)^{\mathrm{T}}.\mathbf{C}_{\mathrm{d}}{}^{-1}.\mathbf{J}_{\mathbf{p}}{}^{post} + \mathbf{C}_{\mathbf{P}_{\mathbf{Prop}}}{}^{-1}\right)^{-1}, \tag{11}$$

where $\mathbf{C}_{\mathbf{P}_{\mathbf{Prop}}}^{post}$ is the posterior covariance matrix and $\mathbf{J}_{\mathbf{p}}{}^{post}$ is the Jacobian matrix of the last iteration step. The diagonal entries of the posterior matrix represent the variances on the property values of each subspace.

3. Validation of the DNDI algorithm on hypothetical study cases

The DNDI inversion algorithm has been tested on three hypothetical and simplified confined karstic fields with network of conduits:

- in a first case, we treat a simple network case with heterogeneity in the equivalent transmissivity of the conduits and a homogenous transmissivity assigned to the matrix,
- a second case is similar to the first one but adding a transmissivity variability also in the matrix,
- in a third case, we seek to image a complex network geometry with the use of two different initial models to start the inverse problem.

We considered in the forward problem (Eq. 1) a unit thickness for the matrix (2D modeling) and a unit aperture for the network (but with a variable equivalent transmissivity). The buffer zone boundaries were associated to a $h_{bound.} = 0$ m Dirichlet condition and the hydraulic heads were set to $h_0 = 0$ m initially over the model. These theoretical study cases were used to produce 2,401 hydraulic drawdown data from 49 pumping/measurement boreholes (a pumping test is performed alternatively in each borehole) distributed homogeneously over the 100×100 m² models. The pumping rates were set to 0.6 L/min for a borehole in the matrix and 5 L/s for one in the conduit network.

In these different cases, for the inversion of the geometry of the network, no a priori information has been added. On the other hand, we have constrained the inversion of the hydraulic properties with a priori values. The a priori models on the properties are used also

as initial model to launch the inversion process. For the property optimization, for the matrix we took the $-\log_{10}(T)$ as transmissivity parameter T_M (for example a transmissivity parameter equal to 6 represents in the model a 10^{-6} m²/s transmissivity value) and for the network we took directly the T value as transmissivity parameter T_N. The covariance matrices $\mathbf{C_d}$ and $\mathbf{C_{P_{Prop}}}$ are built as diagonal matrices with a constant variance value σ^2 (in the case of the matrix transmissivity the variance value $\sigma^2_{T_M}$ applies to the exponent of the transmissivity, in the case of the network transmissivity the variance value $\sigma^2_{T_N}$ applies to the transmissivity). The partitioning of the models and the chosen inversion parameters values for each study case are given in Table 1. The different study cases inversions were led on a 64Go RAM PC on 2 processors of 16 cores.

Table 1: Parameters used in the inversion study cases

	Study case 1	**Study case 2**	**Study case 3**
Partitioning	4x4	4x4	8x8
A priori T_N	0.06 m²/s	0.04 m²/s	0.1 m²/s
A priori T_M	10^{-6} m²/s	10^{-6} m²/s	10^{-6} m²/s
Data cov. matrix $\mathbf{C_d} = \sigma^2_{data}.Id(n)$	$\sigma_{data}=10^{-2}$ m	$\sigma_{data}=10^{-2}$ m	$\sigma_{data}=10^{-2}$ m
Property cov. matrix $\mathbf{C_{P_{Prop}}} = \sigma^2_{T_N/T_M}.Id(2p)$	$\sigma_{T_N}=10^{-6}$ m²/s $\sigma_{T_M}=10^{-6}$	$\sigma_{T_N}=10^{-6}$ m²/s $\sigma_{T_M}=10^{-1}$	$\sigma_{T_N}=10^{-6}$ m²/s $\sigma_{T_M}=10^{-6}$

3.1. Study case 1

In a first study case, we have tested the ability of the inversion method to reproduce a network geometry with variable conduit equivalent transmissivities in a homogeneous matrix. We generated drawdown data from a theoretical model with a 10^{-6} m²/s matrix transmissivity and a principal conduit associated to a 0.1 m²/s transmissivity and secondary conduits associated

to a 0.01 m²/s transmissivity. Firstly we tested an inversion with a small set of data (100 drawdown data from 10 boreholes, see the 'True model' in Figure 5).

We started the inversion from a simple initial model with a single horizontal 0.06 m²/s conduit and a homogeneous 10^{-6} m²/s matrix transmissivity. The structural optimization converged in 10 iterations and the properties optimization in 1 iteration.

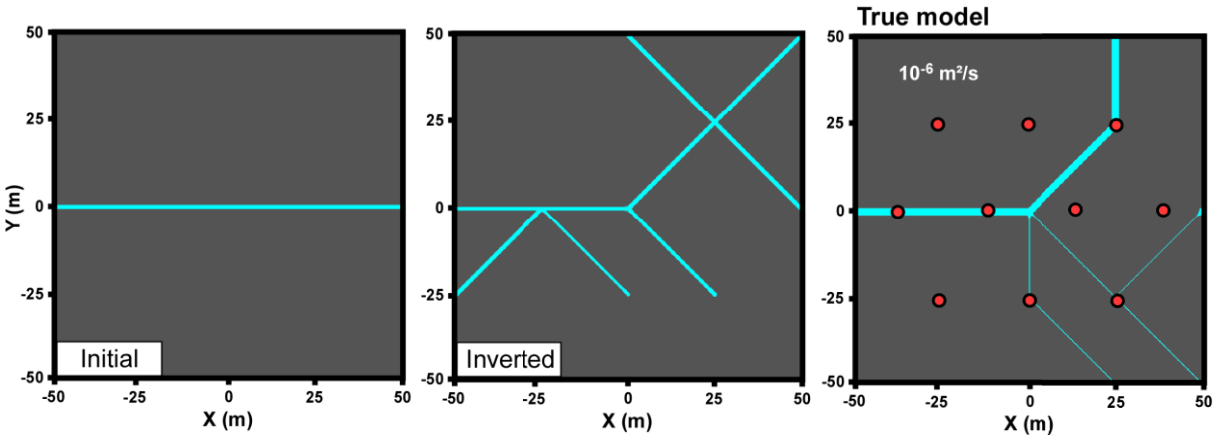

Figure 5: Initial and inverted models for an inversion using drawdown data produced from a true model (on the right) with a homogeneous matrix. The red dots on the true model symbolize the pumping/measurement boreholes for the hydraulic data. The inverted model permits to localize approximatively the karstic network connections but in this case the amount of data is insufficient to have a proper imagery.

The inverted model reproduces the data set (R^2 = 0.97) and approximately the connectivity between the points in the network, however this reconstruction remains distant from the true geometry. This is due to a lack of data to correctly identify the shape of the conduit network. Therefore, the efficiency of the inversion for mapping the heterogeneity of the hydraulic parameters and retrieving the principal karstic conduits is highly dependent to the number of wells and their locations. In the next test, we used a denser distribution of wells (49 wells) for providing a better spatial resolution in order to image the heterogeneity of the aquifer presented for the same 'True model' in Figure 6.

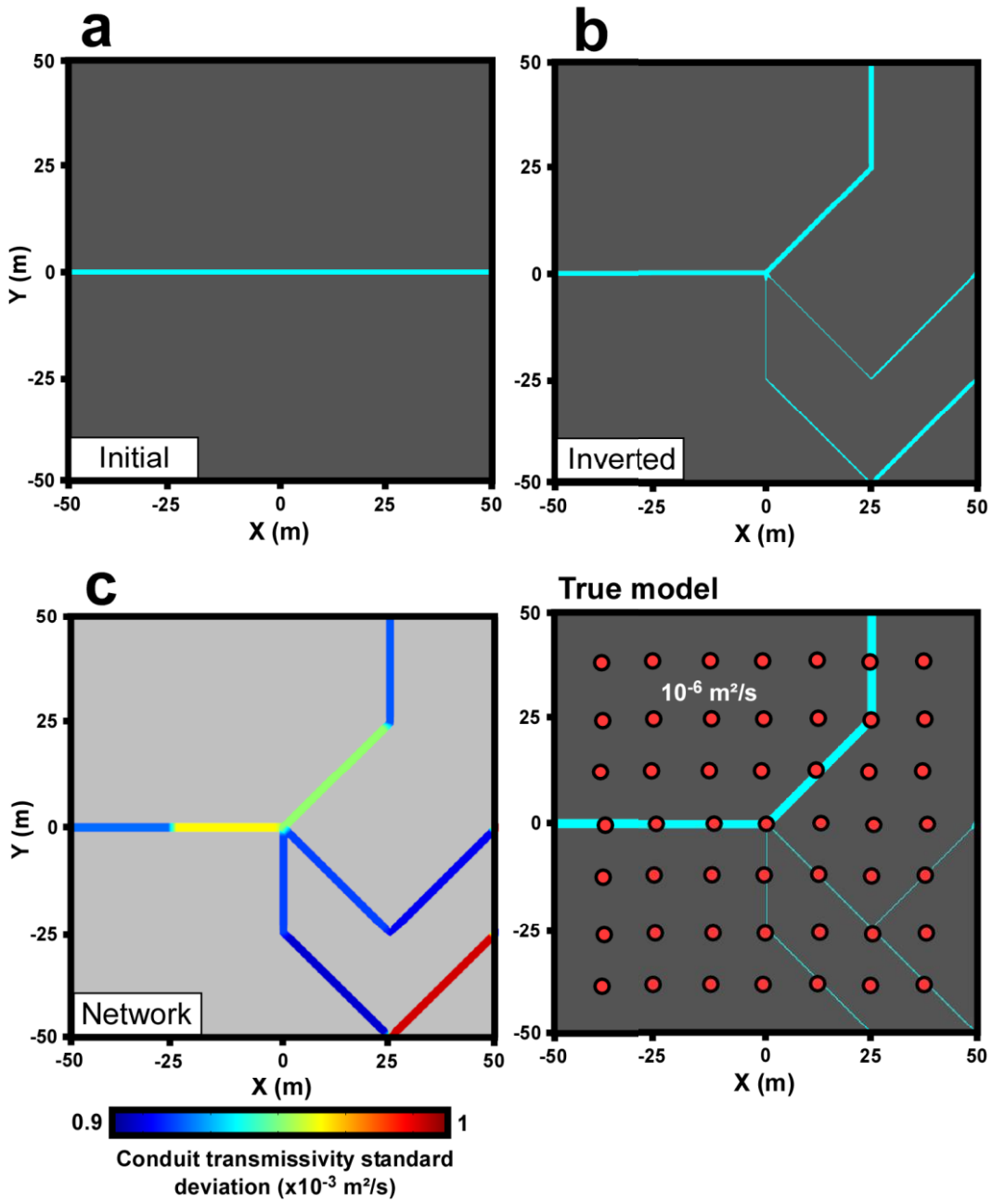

359

360 Figure 6: Initial (a) and inverted (b) models for an inversion using drawdown data produced
361 from a true model with a homogeneous matrix, and associated map of the conduit properties
362 posterior standard deviations (c). The inverted model in (b) permits a good localization the
363 true karstic network. It also reduced locally the initial transmissivity (0.06 m²/s to 0.01 m²/s)
364 of the conduits connected to the primary drain in the bottom right part of the model (the
365 conduit thickness is proportional to its transmissivity value). The red dots on the true model
366 symbolize the pumping/measurement boreholes for the hydraulic data.

367

368 The structural optimization converged in 11 iterations and the properties optimization in 1

369 iteration. The inverted model reproduces now the data set (R^2 = 0.95) and also a very good

representation of the true geometry (Figure 6). The property optimization permitted to correct the initial equivalent transmissivity of 0.06 m²/s to 0.01 m²/s for the conduits connected in the bottom right area of the network. It permits to reduce the flow rates coming to this zone and enhance the reproduction of the true cones of depression. The flows in this zone are mainly conditioned by the properties of the conduits connected directly to the primary drain. This affirmation can be supported by the conduit transmissivity standard deviation map produced from Eq. 11 (Figure 6), that shows that the properties of the conduits directly connected to the primary drain have lower uncertainties than the primary drain itself in the center of the inverted model. The conduit in the bottom right periphery of the inverted model does not image correctly the true model. But as the data reproduction is perfect, this periphery zone might not be sufficiently described by the data to permit a very good reproduction. The uncertainty map confirms that this part of the network has a more uncertain transmissivity value than the rest of the network.

We have also tested another configuration with more available boreholes than in the case in Figure 5, but in which only two boreholes intersect the true karstic network. The true model and the inversion result are presented in Figure 7.

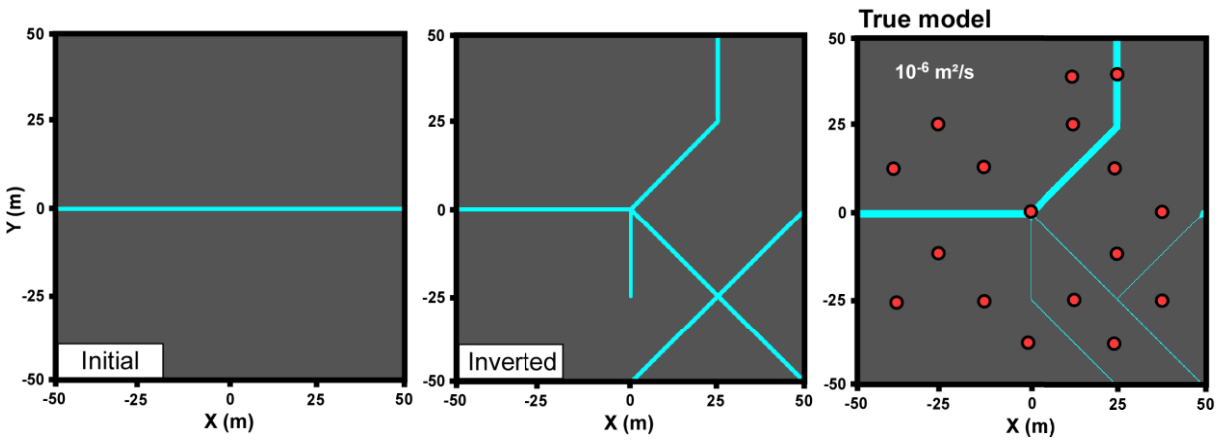

Figure 7: Initial and inverted models for an inversion using drawdown data produced from a true model (on the right) with a homogeneous matrix. The red dots on the true model symbolize the pumping/measurement boreholes for the hydraulic data, primarily located in

390 the matrix. The inverted model permits to almost reproduce the karstic network even if only
391 two measurement points are located in the true network.

392

393 The inverted model can almost reproduce the true network geometry, which shows that
394 boreholes, even in the matrix, can provide information about the localization of nearby
395 conduits. This is especially true for the thin conduits which appear in the inverted model
396 although no boreholes are intersecting them. Therefore the DNDI method can be used with
397 dataset with only a few boreholes intersecting the conduits as long as there are a sufficient
398 number of other boreholes, in the matrix, in suitable locations for characterizing the nearby
399 conduit network.

400 ## 3.2. Study case 2

401 A second study case was led to test the ability of this inversion method to reproduce the data
402 in a case of a karstic network with various conduit properties developed in a heterogeneous
403 matrix. We simulated the piezometric data from a theoretical model with the same karstic
404 network than in study case 1, but in a matrix with a transmissivity varying from 5.10^{-6} m²/s to
405 5.10^{-7} m²/s (Figure 8).

406 We started the inversion from a simple initial model with a single horizontal 0.04 m²/s conduit
407 and a homogeneous 10^{-6} m²/s matrix transmissivity. The structural optimization converged in
408 10 iterations and the properties optimization in 3 iterations (Figure 8a).

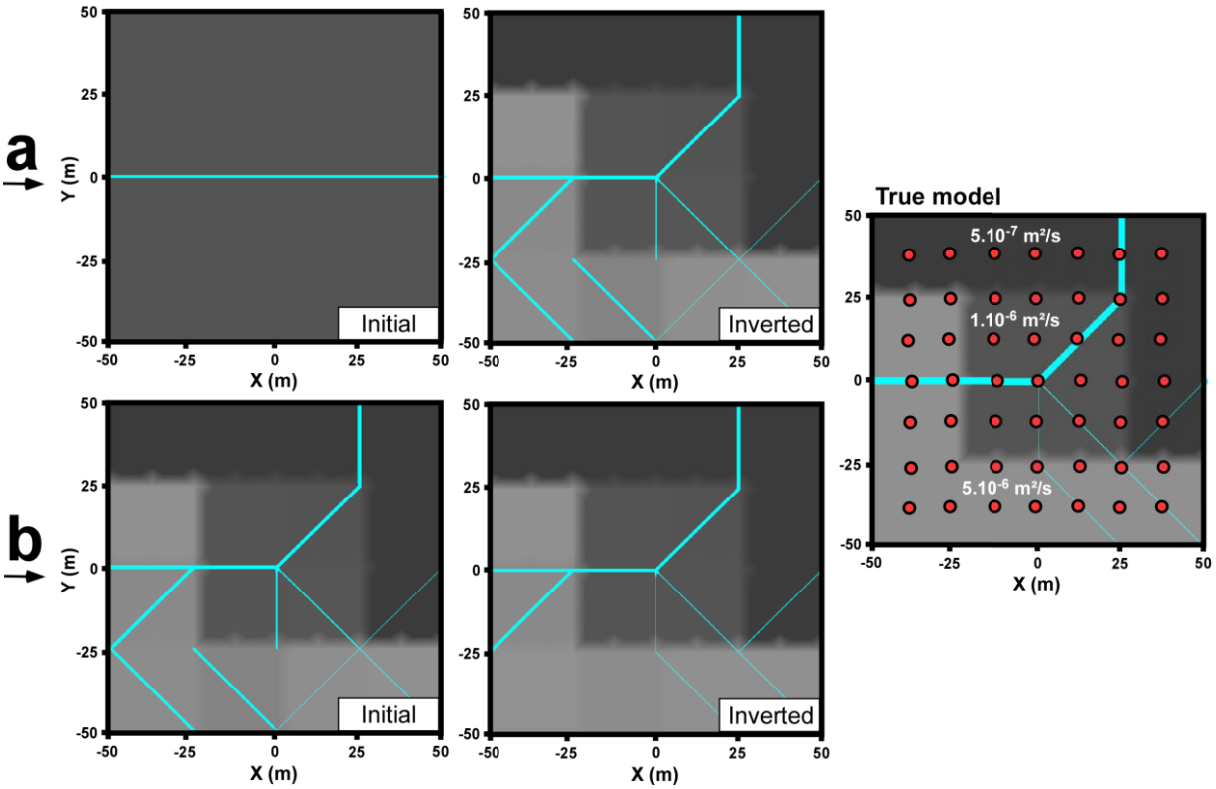

409

410 Figure 8: Initial and inverted models for an inversion using drawdown data produced from a
411 true model (on the right) with a heterogeneous matrix. The red dots on the true model
412 symbolize the pumping/measurement boreholes for the hydraulic data. A first inverted model
413 (a) permits to localize the true karstic network but also generates conduits to simulate the
414 more transmissive part of the true model. A second inversion (b) starting from the previous
415 inverted model permits to correct the geometry and produces an inverted model matching
416 more accurately the true model.

417

418 The structural optimization permitted to retrieve the true geometry of the conduits network,
419 but it also added conduits in the bottom left part of the model to reproduce the drawdown data
420 of the more transmissive area of the matrix. Then the property optimization could reproduce
421 the true transmissivity values distribution in the matrix. In the end the inverted model can
422 reproduce the true drawdowns data, but its network geometry incorporates parts, inexistent in
423 the true model, that has been generated in order to simulate a more transmissive area of the
424 matrix before the matrix transmissivity values could be optimized.

425 We started a second inversion using the previously inverted model (indicated in Figure 4 as
426 the 'multi-scale option'). The structural optimization converged in 2 iterations and the

parameter property optimization in 1 iteration (Figure 8b). The only changes were made during the structural optimization step, with an important improvement in the identification of the shape of the conduits. In this case the inverted model reproduces the drawdowns data (R^2 = 0.99) but is also a good representation of the true network geometry.

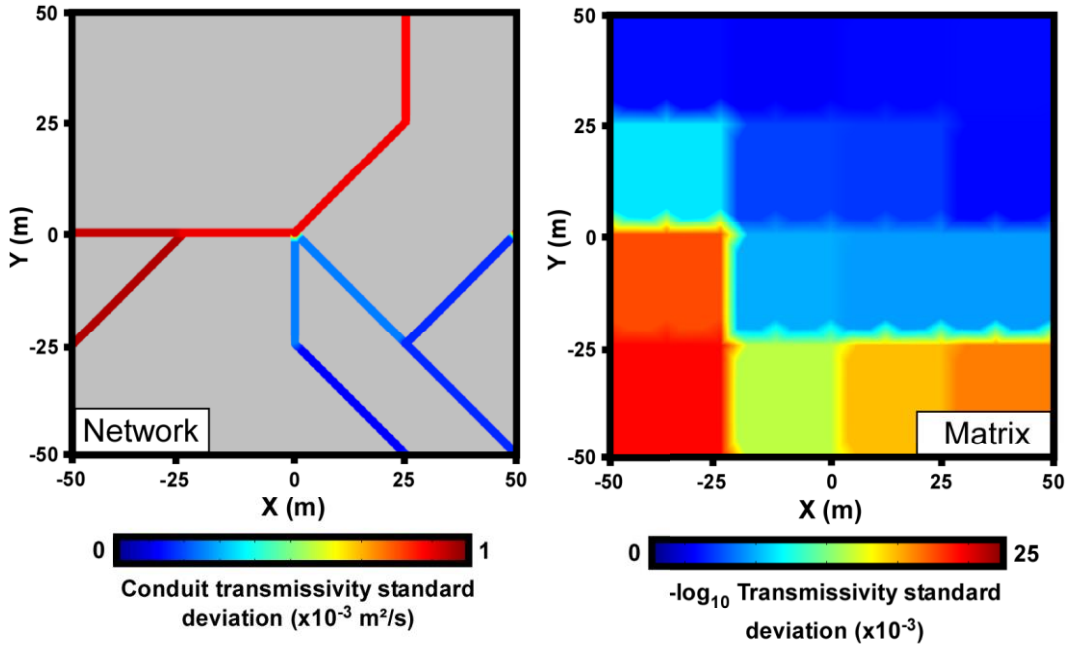

Figure 9: Maps of the conduit and matrix transmissivities posterior standard deviations. The matrix higher transmissivity zones in the inverted model (bottom left) have a higher uncertainty value than the lower transmissivity zones (top right). On the contrary, the uncertainty on the transmissivities of the conduits of the primary drain is higher than the secondary conduits.

The posterior standard deviation maps produced from Eq. 11 (Figure 9) show, for the conduit property values, a smaller uncertainty for the secondary conduits and a higher uncertainty for the primary drain, especially for the part of the network on the left of the model. Concerning the matrix transmissivity property values, the highest uncertainty are located mostly in the most transmissive areas.

3.3.Study case 3

Finally, a third study case was led to test the ability of this inversion method to reproduce the data in a case of a complex karstic network geometry. We generated drawdown data from a theoretical model with a karstic network with a constant equivalent transmissivity of 0.1 m^2/s in a homogeneous matrix with a transmissivity of 10^{-6} m^2/s (Figure 10).

We started an inversion from a simple initial model with a single vertical 0.1 m^2/s conduit and a homogeneous 10^{-6} m^2/s matrix transmissivity. The structural optimization converged in 33 iterations and the parameter optimization in 1 iteration (Figure 10a). The inverted model permits to fit the data set approximately ($R^2 = 0.78$) and represents the global geometry of the conduits network of the true model. Regarding the simplicity of the initial model, the result model remains satisfying.

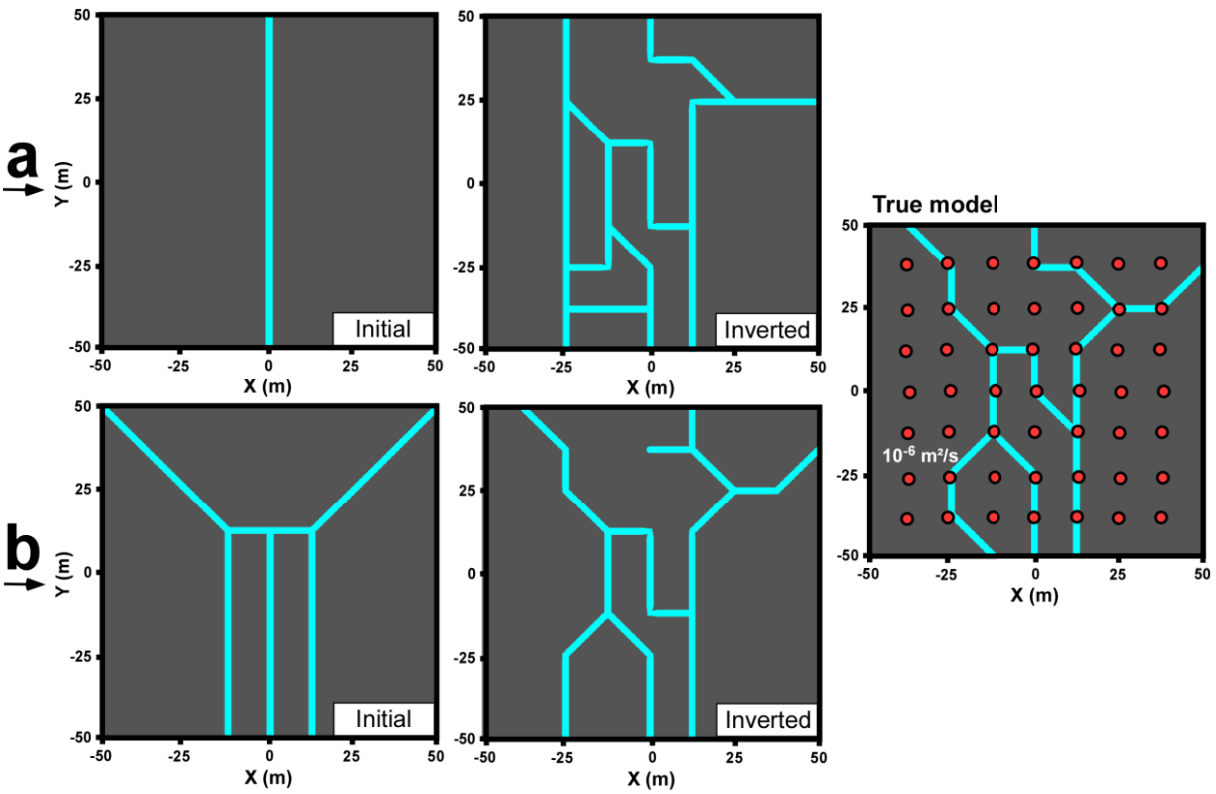

Figure 10: Initial and inverted models for an inversion using drawdown data generated from a true model (on the right) with a homogeneous matrix. The red dots on the true model symbolize the pumping/measurement boreholes for the hydraulic data. A first inverted model (a), starting from a simple initial model, permits to localize approximately the true network geometry. A second inversion (b), starting from a more detailed initial model, permits to produce a more precise network geometry.

We also started an inversion from a more complex initial model with two vertical 0.1 m²/s conduits diverging in the upper part of the model in a homogeneous 10^{-6} m²/s matrix transmissivity. This initial model geometry (representing a simple approximation of the true geometry) can be associated to a priori field knowledge information. The structural optimization converged in 17 iterations and the parameter optimization in 1 iteration (Figure 10b). In this case, the inverted geometry of the discrete network permits a good reproduction of the data ($R^2 = 0.97$) and is closer to the real network than the case in Figure 10a.

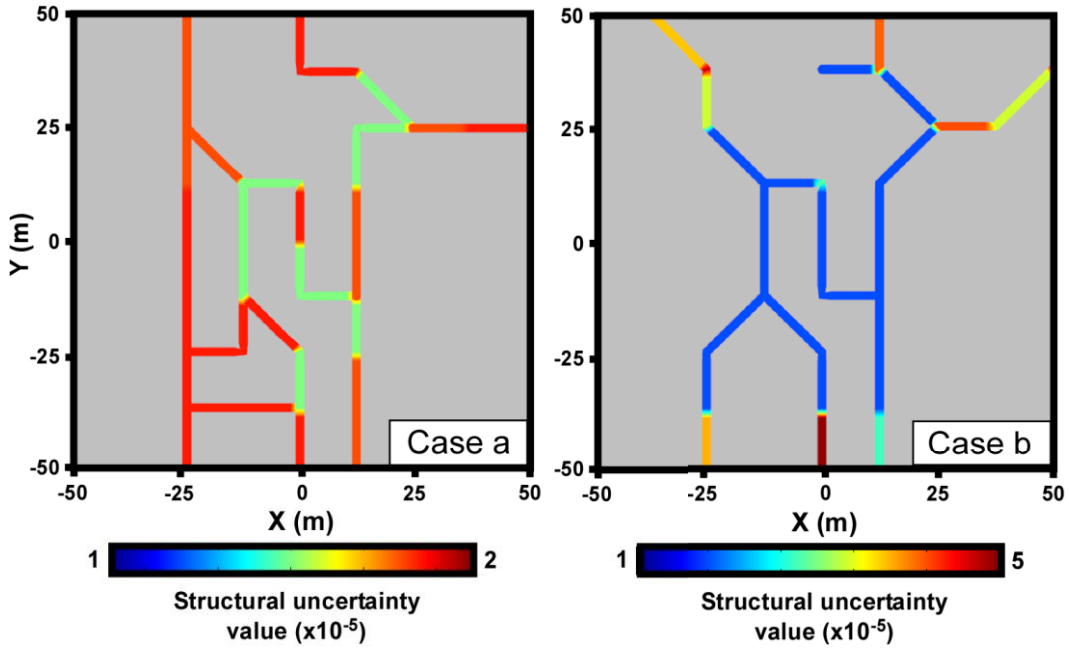

Figure 11: Maps of the posterior uncertainties of the network local directions for the Cases a and b. In the Case a, started from a simple initial model, the highest uncertainties are distributed uniformly over the inverted network. In the Case b, started from a more detailed initial model, the highest uncertainties are located in the periphery of the model.

The structural posterior uncertainty maps produced from Eq. 8 are presented in Figure 11. These maps show that, in the Case a, the highest uncertainties are distributed relatively uniformly among the inverted model, while in Case b, they are mostly located in the periphery

of the model. Here, the structural posterior uncertainties are giving important information about the local validity of the different inverted networks.

4. Discussion

We have successfully tested the DNDI method on three theoretical and simplified study cases with steady state drawdowns. However as we have seen, an inversion process is limited by the non-uniqueness of its solution. Therefore using the DNDI method requires several prerequisites and the modeler needs to be critical toward the result.

As we have seen in the first study case, the efficiency of the inversion is dependent to the hydraulic data set, and in particular the number and the localization of observation wells on the field. We note that even wells in the matrix can provide information on nearby conduits for the inversion. Globally it appears that the most important point about a steady-state dataset is to have a homogeneous and sufficiently dense distribution of wells on the site, in order to characterize successfully the network.

Concerning the inversion process itself, we note, in the third study case, the ability of the DNDI method to image complex networks. However, as the inversion is deterministic, the precision of the result model is dependent to the initial model. The inversion process will converge to a local solution dependent to the initial model. In fact, in Figure 10 we show that a simple initial model permitted to reproduce a satisfying global representation of the true model, but with local approximations, while a more complex initial model permitted a more accurate reproduction of the true model and a faster convergence. Therefore an inverted model using the DNDI method should be analyzed critically, like any deterministic inverse methods, depending from the initial model. The study of the computed structural and property uncertainty values (with Eq. 8 and Eq. 11) can supply this critical analysis on the result model.

The second study case also illustrates some limits of the sequential optimization of the method, especially when starting from a too simple initial model. Therefore the amount of a priori information introduced in the initial model is important for the accuracy of the result model. Otherwise, as we demonstrate in Figure 8, a simple possible operation would be to re-run the inversion with a first inversion result to slightly improve the result. We would also recommend the coupling of this inversion method to a multiscale method (Grimstadt et al. 2003) which consists in a re-run of the inversion starting from a previous result with a refinement of the partitioning. It permits to lead several inversions with an initial model each time more precise while saving time as we initially start with a coarsely partitioned model.

5. Conclusion

We present in this paper a novel deterministic inversion method that permits to characterize, in a partitioned model, the karst conduits and fractures network geometry and their hydraulic properties, including the transmissivity distribution of the matrices. The DNDI method let the modeler choose the partitioning of the model for the inversion. This ‘cursor’ permits to define either an inversion with a coarse partitioning for a quick approximation model, or with a fine partitioning and a longer computation time for a better fitting model. The use of a discrete network model permits to associate a specific behavior to the flows in the network and thus, produces more realistic models than an equivalent porous media model. This method can be easily adapted for channels or fractures network models by modifying the properties associated to the discrete network (these properties can also be directly linked to an aperture value, by choosing an adapted law). Therefore we believe that the DNDI method is an interesting new imagery tool for the distributed modeling associated to a set of data from an investigation in a karstic and/or fractured aquifer.

525 We have realized different tests in three theoretical and simplified study cases with an
526 increasing complexity, and the DNDI could always produce satisfying results, both on the
527 reproduction of the generated data and on finding the network geometry and property values
528 from the true model. As we have seen in the first study case, the result of the structural
529 inversion is dependent on the positioning and the amount of observed data. This is true for
530 any inversion, but is especially important in the case of highly heterogeneous aquifers for
531 delineating the position of the heterogeneities. Therefore, the result of the inversion has to be
532 interpreted critically regarding the set of data used for it. A first critical analysis can be
533 performed from the maps of posterior uncertainties on the structure or on the property values
534 that can be produced by using the formulas we propose in this paper. The a priori information
535 on the geometry of the network and on the property values is also a way to constrain the
536 inversion in addition to the data. This information can be inferred from general field
537 knowledges (geological and geophysical information, conduits observation in wells through
538 video camera, other studies, etc.)

539 Because this method is deterministic, the choice of the initial model should be based on a
540 relatively coherent possibility and should not be too far from the real solution in order to
541 produce a good result. Therefore, we propose to couple the DNDI method to a multi-scale
542 method. This consists in a first inversion started from an initial model which is followed by a
543 new one that starts from the first inversion solution with a refined partitioning. This strategy
544 permits to start from a simple initial model and to progressively make the model more
545 complex and improve the solution.

546 An application of this method for mapping the conduits and fractures network with real data
547 from a karstic field is planned for future works. These works will be more specifically
548 focused on the sensitivity of the method to the spatial distribution of the measurement
549 boreholes and on delineating the preferential flow paths in the network.

Acknowledgments

We thank the Normandy region for providing financial support for the PhD of Pierre Fischer. We also would like to thank two anonymous reviewers for their contribution to the improvement of this article.

References

Ackerer, P., F. Delay. 2010. Inversion of a set of well-test interferences in a fractured limestone aquifer by using an automatic downscaling parameterization technique. *Journal of Hydrology* 389: 42-56.

Bonneau, F., V. Henrion, G. Caumon, P. Renard, J. Sausse. 2013. A methodology for pseudo-genetic stochastic modeling of discrete fracture networks. *Computer & Geosciences* 56: 12-22.

Borghi, A., P. Renard, F. Cornaton. 2016. Can one identify karst conduit networks geometry and properties from hydraulic and tracer test data? *Advances in Water Resources* 90: 99-115.

Butler, J.J. 2005. Hydrogeological methods for estimation of spatial variations in hydraulic conductivity. In: Rubin, Y., S.S. Hubbard. Hydrogeophysics. *Water Science and Technology Library* (vol. 50). Springer, Dordrecht.

Caers, J. and T. Hoffman. 2006. The probability perturbation method: A new look at Bayesian inverse modeling. *Mathematical Geology* 38 (No. 1): 81-100.

Carrera, J., A. Alcolea, A. Medina, J. Hidalgo, L.J. Slooten. 2005. Inverse problem in hydrogeology. *Hydrogeology Journal* 13 (No. 1): 206-222.

576 Cliffe, K., D. Holton, P. Houston, C. Jackson, S. Joyce, A. Milne. 2011. Conditioning discrete
577 fracture network models of groundwater flow. *International Journal of Numerical Analysis*
578 *and Modeling* 8 (No. 4): 543-565.

579

580 Collon, P., D. Bernasconi, C. Vuilleumier, P. Renard. 2017. Statistical metrics for the
581 characterization of karst network geometry and topology. *Geomorphology* 283: 122-142.

582

583 De Rooij, R., P. Perrochet, W. Graham. 2013. From rainfall to spring discharge: coupling
584 conduit flow, subsurface matrix flow and surface flow in karst systems using a discrete-
585 continuum model. *Advances in Water Resources* 61: 29-41.

586

587 Eisenlohr, L., L. Kiraly, M. Bouzelboudjen, Y. Rossier. 1997. Numerical simulation as a tool
588 for checking the interpretation of karst spring hydrographs. *Journal of Hydrology* 193: 306-
589 315.

590

591 Fischer, P., A. Jardani, N. Lecoq. 2017. A cellular automata-based deterministic inversion
592 algorithm for the characterization of linear structural heterogeneities. *Water Resources*
593 *Research* 53: 2016-2034.

594

595 Ghasemizadeh, R., F. Hellweger, C. Butscher, I. Padilla, D. Vesper, M. Field, A.
596 Alshawabkeh. 2012. Review: Groundwater flow and transport modeling of karst aquifers,

with particular reference to the North Coast Limestone aquifer system of Puerto Rico. *Hydrogeology Journal* 20: 1441–1461.

Grimstadt, A.-A., T. Mannseth, G. Naevdal, H. Urkedal. 2003. Adaptive multiscale permeability estimation. *Computers & Geosciences* 7 (No. 1):1-25.

Hao, Y., T.-C.J. Yeh, J. Xiang, W.A. Illman, K. Ando, K.-C. Hsu, C.-H. Lee. 2008. Hydraulic tomography for detecting fracture zone connectivity. *Ground Water* 46: 183–192.

Hartmann , A., N. Goldscheider, T. Wagener, J. Lange, M. Weiler. 2014. Karst water resources in a changing world: review of hydrological modeling approaches. *Reviews of Geophysics* 52 (No. 3): 218-242.

Illman, W.A., X. Liu, S. Takeuchi, T.-C.J. Yeh, K. Ando, H. Saegusa. 2009. Hydraulic tomography in fractured granite: Mizunami underground research site, Japan. *Water Resources Research* 45 doi: 10.1029/2007WR006715.

Illman, W.A. 2014. Hydraulic tomography offers improved imaging of heterogeneity in fractured rocks. *Groundwater* 52 (No. 5): 659-684.

Jaquet, O., P. Siegel, G. Klubertanz, H. Benabderrhamane. 2004. Stochastic discrete model of karstic networks. *Advances in Water Resources* 27: 751-760.

Kovacs, A. 2003. Estimation of conduits network geometry of a karst aquifer by the means of groundwater flow modeling (Bure, Switzerland). *Boletin Geologico y Minero* 114 (No. 2): 183-192.

Kovacs, A., P. Perrochet, L. Kiraly, P.-Y. Jeannin. 2005. A quantitative method for the characterization of karst aquifers based on spring hydrograph analysis. *Journal of Hydrology* 303: 152-164.

Larocque, M., O. Banton, P. Ackerer, M. Razack. 1999. Determining karst transmissivities with inverse modeling and an equivalent porous media. *Ground Water* 37 (No. 6): 897-903.

Lavenue, M., G. de Marsily. 2001. Three-dimensional interference test interpretation in a fractured aquifer using the pilot point inverse method. *Water Resources Research* 37 (No. 11): 2659-2675.

Le Coz, M., J. Bodin, P. Renard. 2017. On the use of multiple-point statistics to improve groundwater flow modeling in karst aquifers: a case study from the hydrogeological experimental site of Poitiers, France. *Journal of Hydrology* 545: 109-119.

639 Le Goc, R., J.-R. de Dreuzy, P. Davy. 2010. An inverse problem methodology to identify
640 flow channels in fractured media using synthetic steady-state head and geometrical data.
641 *Advances in Water Resources* 33: 782-800.

642

643 Li, Z.Y., J.H. Zhao, X.H. Qiao, Y.X. Zhang. 2014. An automated approach for conditioning
644 discrete fracture network modelling to in situ measurements. *Australian Journal of Earth*
645 *Sciences* 61: 755-763.

646

647 Liedl, R., M. Sauter, D. Huckinghaus, T. Clemens, G. Teutsch. 2003. Simulation of the
648 development of karst aquifers using a coupled continuum pipe flow model. *Water Resources*
649 *Research* 39, 1057.

650

651 Meier, P., A. Medina, J. Carrera. 2001. Geostatistical inversion of cross-hole pumping tests
652 for identifying preferential flow channels within a shear zone. *Groundwater* 39 (No. 1): 10-
653 17.

654

655 Ni, C.-F., T.-C.J. Yeh. 2008. Stochastic inversion of pneumatic cross-hole tests and
656 barometric pressure fluctuations in heterogeneous unsaturated formations. *Advances in Water*
657 *Resources* 31: 1708-1718.

658

659 Painter, S., V. Cvetkovic. 2005. Upscaling discrete fracture network simulations: An
660 alternative to continuum transport models. *Water Resources Research* 41
661 doi:10.1029/2004WR003682.

662

663 Pardo-Iguzquiza, E., P.A. Dowd, C. Xu, J.J. Duran-Valsero. 2012. Stochastic simulation of
664 karst conduit networks. *Advances in Water Resources* 35: 141-150

665

666 Ronayne, M.J. 2013. Influence of conduit network geometry on solute transport in karst with
667 a permeable matrix. *Advances in Water Resources* 56: 27-34.

668

669 Sharmeen, R., W.A. Illman, S.J. Berg, T.-C.J. Yeh, Y.-J. Park, E.A. Sudicky, K. Ando. 2012.
670 Transient hydraulic tomography in a fractured dolostone: laboratory rock block experiments.
671 *Water Resources Research* 48 doi: 10.1029/2012WR012216.

672

673 Soueid Ahmed, A., J. Zhou, A. Jardani, A. Revil, J. Dupont. 2015. Image-guided inversion in
674 steady-state hydraulic tomography. *Advances in Water Resources* 82: 83-97.

675

676 Tarantola, A. and B. Valette. 1982. Generalized nonlinear inverse problems solved using the
677 least squares criterion. *Reviews of Geophysics and Space Physics* 20 (No. 2): 219-232.

678

679 Teutsch, G. 1993. An extended double-porosity concept as a practical modeling approach for
680 a karstified terrain. *Hydrogeological Processes in Karst Terranes* 207: 281-292.

Wang, X., A. Jardani, H. Jourde, L. Lonergan, J. Cosgrove, O. Gosselin, G. Massonat. 2016. Characterisation of the transmissivity field of a fractured and karstified aquifer, Southern France. *Advances in Water Resources* 87:106-121.

Wang, X., A. Jardani, H. Jourde. 2017. A hybrid inverse method for hydraulic tomography in fractured and karstic media. *Journal of Hydrology* 551: 29-46.

Yeh, T.-C.J., S. Liu. 2000. Hydraulic tomography: development of a new aquifer test method. *Water Resources Research* 36 (No. 8): 2095-2105.

Yeh, T.-C.J., C.-H. Lee. 2007. Time to change the way we collect and analyze data for aquifer characterization. *Groundwater* 45 (No. 2): 116-118.

Zhou, H., J. Gomez-Hernandez, L. Li. 2014. Inverse methods in hydrogeology: evolution and recent trends. *Advances in Water Resources* 63: 22-37.